Journal of the European Ceramic Society xxx (xxxx) xxx–xxx

Contents lists available at ScienceDirect

Journal of the European Ceramic Society

journal homepage: www.elsevier.com/locate/jeurceramsoc

Original Article

Comparative study of surface properties of Mg-substituted hydroxyapatite bioceramic microspheres

Liga Stipniece[a,*], Valentina Stepanova[a], Inga Narkevica[a], Kristine Salma-Ancane[a], Adrian R. Boyd[b]

[a] Rudolfs Cimdins Riga Biomaterials Innovations and Development Centre of RTU, Institute of General Chemical Engineering, Faculty of Materials Science and Applied Chemistry, Riga Technical University, Pulka 3, Riga, LV-1007, Latvia

[b] Nanotechnology and Integrated Bioengineering Centre (NIBEC), School of Engineering, Ulster University, Shore Road, Newtownabbey, Co. Antrim, BT37 0QB, Northern Ireland, UK

ARTICLE INFO

Keywords:
Hydroxyapatite
Bioceramic
Microspheres
Mg substitution
Protein adsorption

ABSTRACT

Mg-substituted hydroxyapatite (HAp) bioceramic microspheres were prepared by spray drying and subsequent processing at 1173, 1273 and 1373 K. Influence of various Mg substitution levels (up to 0.84 ± 0.10 wt%) on physicochemical properties of the HAp bioceramic microspheres was evaluated. Obtained results were used for the elucidation of the compositional and structural characteristics of the microspheres in conjunction with adsorption of protein, namely, bovine serum albumin (BSA). The primary difference among the microspheres processed at various temperature was the presence or absence of the micropores (< 2 nm in diameter) and mesopores (between 2 and 50 nm). Presence of the micro- and mesopores resulted in higher specific surface area (SSA), enhanced solubility, *i.e.*, ion release, and, accordingly, increase in the amount of BSA adsorbed on the microspheres. Furthermore, the BSA adsorption capacity of the microspheres decreased with increasing Mg content despite of higher SSA.

1. Introduction

The continuously increasing demand to improve life quality concerns an innovative use of specifically designed biomaterials for the repair and reconstruction of diseased or damaged bones. Nowadays the focus has shifted towards bone replacement and repair materials that can mimic living tissues (biomimetic) and assist in the healing process (*i.e.*, be replaced by natural bone): thus, they are bioactive [1]. The most commonly used biomaterials for such applications include calcium phosphates (CaP) [2]. The use of CaP, particularly hydroxyapatite (HAp, $Ca_{10}(PO_4)_6(OH)_2$), for the repair or regeneration of diseased or damaged bone tissues is based generally on the chemical and structural similarity to a mineral component of bone, namely, biological HAp [1,2].

Biological HAp contains various ionic substitutions resulting in a multi-element substituted material [3]. Consequentially, due to their essential functions in many important biological processes, including bone formation, remodelling and metabolism, various biologically active mineral elements have become important bone graft additives for enhanced bone regeneration and repair [4]. Therefore, the most recent studies in the field of bone grafting materials, particularly HAp, have been focused on control of chemical composition in order to optimise bioresorbability and bioactivity, as well as to impart specific properties [5]. As such, a wide range of elements, including, Mg [6,7], Sr [7,8], Zn [8], Ag [9] *etc.* have been strategically incorporated intostructure of synthetic HAp. It has been reported that through several types of substitutions in HAp lattice various properties such as crystal structure (crystallite size and crystallinity), phase and thermal stability and solubility, and adsorption (surface reactivity) can be customized for specific application [3,10].

Among other cationic substitutions for Ca in HAp lattice, in the present study Mg was chosen as it is essential trace element in human bone [11]. Above all, having the optimum amount of Mg in relation to Ca is critical for preventing and reversing osteoporosis [12]. Mg is known to promote cellular adhesion onto the substrate, and is also known to enhance osteoblast-like cell proliferation and differentiation, calcification and angiogenic functions [13]. Thus, incorporation of Mg into the synthetic HAp is important for a number of reasons, including, enhance of bioactivity [14]. In this study relatively low levels, namely close to bone-like amounts (up to 1 wt%) of Mg substitution were chosen due to the potential cytotoxicity of high local concentrations of Mg at site of implantation [15].

* Corresponding author.
E-mail addresses: liga.stipniece@rtu.lv, ligastipniece@inbox.lv (L. Stipniece).

http://dx.doi.org/10.1016/j.jeurceramsoc.2017.09.026
Received 7 July 2017; Received in revised form 14 September 2017; Accepted 17 September 2017

Porous HAp biomaterials have found to stimulate bone formation and bone bonding, which is related to the specific interactions, *e.g.* ionic exchanges, of their surface with the extracellular fluids [16,17]. Among others, HAp in the form of microspheres has been widely investigated for their potential as local drug- or protein- delivery systems. Furthermore, the microspheres with porous structure provide a high surface area not only for protein adsorption but also cell attachment [18]. The microspheres having capacity to entrap wide range of active ingredients such as drugs and proteins, are used as the topical carrier systems. The microspheres loaded with active ingredients can be incorporated into formulations such as gels, bone cements *etc*. One of the most widely applied techniques to prepare microspheres is spray drying due to its simplicity, the particle size can be controlled in a single step and can be scaled up to ton quantities [19]. The wide use of HAp microspheres is typical 10, 20, 40, and 80 μm in size [20]. However, there are many advantages of reducing size of the microspheres. Mainly, reduced size of the individual particles leads to higher surface area of the compound and, thus, to higher bonding capacity of biomolecules, including proteins [21].

Various proteins have been therapeutically used for the treatment of metabolic disorders and to aid the healing and regrowth of tissues/organs. Thus, a substantial amount of research is focused on effectively delivering these proteins locally to the defective/diseased tissues or organs where they may accelerate or aid the healing process [22]. Moreover, it has been reported that when the bioceramic bone grafts are implanted into a living body, proteins from the surrounding body fluids are spontaneously adsorbed onto their surfaces, and then cellular attachment, proliferation and migration occurs. Summarizing the above-mentioned and considering the widely reported ion-protein interactions, it can be anticipated that HAp have the appropriate properties for protein delivery applications in bone therapeutics [23].

HAp contains two types of binding sites for proteins–positively charged Ca^{2+} and negatively charged $PO_4{}^{3-}$. These sites are distributed regularly throughout the crystal structure of the matrix [20]. Considering the abovementioned effect of substituting elements on the HAp properties, substituting Ca, [PO_2] and/or [OH] in the lattice, should result in significant effects for interaction with proteins. Nevertheless, the effect of Mg as well as the ensuing surface properties of the HAp bioceramic microspheres on the loading profile of the proteins has not been emphasized to the best of available literature. Thus, the objective of this study is to elucidate the connection between the related factors, such as specific surface area, pore size distribution, and solubility (*i.e.*, ion release) with the adsorption capacity of proteins (*i.e.*, bovine serum albumin (BSA) as a model protein) on Mg-substituted HAp bioceramic microspheres.

2. Materials and methods

2.1. Sample preparation

Microspheres were prepared by a spray drying method using a table-top spray dryer (Mini Spray Dryer B-290, Büchi, Switzerland). The 0.03 M slurries for spray drying were obtained by precipitating Mg-susbtituted HAp nanoparticles with a (Ca + Mg)/P molar ratio of 1.67, as described in detail elsewhere [6]. The conventional aqueous precipitation method based on an acid-base reaction involving CaO (puriss.; Fluka, Switzerland) and H_3PO_4 (puriss.; 75%, Sigma-Aldrich, Germany) was modified for Mg precursor, namely MgO (reagent-grade; ES/Scharlau, Spain), addition into the synthesis media. Various concentrations of Mg in the products were provided by changing amount of MgO added into synthesis media. The MgO content in the synthesis media varies from 0 wt% to 3 wt% in respect to a Ca source, namely CaO. After aging for ~20 h, the precipitated slurry underwent spray drying by exploiting conditions, which are summarized in Table 1.

The obtained (as-dried) microspheres were sintered at 1173 K for 1 h, 1273 K for 1 h or 1373 K for 1 h in a muffle furnace using a heating/cooling rate of 5 K/min.

Table 1
Spray drying conditions.

Diameter of nozzle, mm	Inlet temperature, K	Outlet temperature, K	Feed flow rate, L/h	Atomization gas (air) flow, L/h
1.5	493	353 ± 5	0.3	246–357

2.2. Physicochemical characterization

Chemical constitutions of the as-dried and sintered microspheres were determined by energy dispersive X-ray spectrometry (EDX; Mira/LMU/Inca Energy 350, Tescan, Czech Republic).

Molecular composition of the sintered microspheres was determined by Fourier transformation infrared spectroscopy (FT-IR; Varian 800, Scimitar Series, USA) using GladiATR™ (Pike Technologies, USA) single reflection attenuated total reflectance (ATR) accessory utilizing a monolithic diamond crystal. Spectra were recorded in the range of 400–4000 cm^{-1} with spectral resolution of 4 cm^{-1} and 50 spectra were co-added. Prior every measurement a background spectrum was taken and deducted from the sample spectrum.

Phase composition of the sintered microspheres was analyzed by X-ray diffractometer system (XRD; X'Pert PRO, PANalytical, Netherlands) operating at 40 KV and 30 mA using a Cu $K\alpha_1$ radiation (λ = 1.5406 Å). Scans were recorded over the range of 2θ from 10° to 70° with an angular step interval of 0.0334°. For the phase identification the International Centre for Diffraction Data (ICDD) was used (card #01-072-1243 for HAp, card #00-009-0169 for β-tricalcium phosphate (β-TCP)).

Sintering behaviour of the as-dried microspheres was investigated by high-temperature optical dilatometer (EM201/HT163, Hesse Instruments, Germany) using following methodology: the powders weighing ~20 mg were compressed into a cylindrically shaped pellets and heated to 773 K at heating rate 80 K/min, and further to 1623 K at heating rate 15 K/min.

Microstructural features of the sintered microspheres were studied by field emission scanning electron microscopy (FE-SEM; Mira/LMU, Tescan, Czech Republic) at acceleration voltage of 30 kV and distance of 10 mm. Samples were sputter coated with thin (15 nm) gold layer. Average diameter of the microspheres was determined using VEGA TC software, measuring at least 100 objects in FE-SEM micrographs for each batch.

The *Brunauer–Emmett–Teller* (BET) method was used to determine specific surface area (SSA) of the as-dried and sintered microspheres by measuring the amount of physically adsorbed N_2 gas at 76 K (Quadrasorb-SI Kr, Quantachrome, USA). The samples were degassed at 373 K for 2 h prior the analyses. The pore size distribution in a range of 0–30 nm were derived from the adsorption branches of the isotherms using density functional theory (DFT).

2.3. Ion release

Solubility, namely cumulative release of Ca^{2+} was determined by placing the Mg-substituted HAp microspheres (200 mg) in tris(hydroxymethyl)aminomethane (TRIS; ACS reagent, ≥99.8%, Sigma Aldrich, USA) and hydrochloric acid (HCl; 37%, Sigma Aldrich, USA) buffer pH 7.4 ± 0.2 (50 mL) at 310 K for 168 h in a table-top environmental shaker-incubator (ES-20, Biosan, Latvia) providing mild, orbital shaking at 70 RPM. TRIS–HCl solution was prepared according to the EN ISO 10993-14:2001. Every 24 h the microspheres were sediment by centrifugation at 3000 RPM for 1 min, "reacted" TRIS–HCl was removed and the microspheres were re-suspended in fresh TRIS–HCl up to

total volume 50 mL. "Reacted" solutions were used to measure Ca^{2+} concentrations by complexometric titration with 0.01 M EDTA using automated titrator (T 90, Mettler Toledo, USA) and Ca ion-selective electrode (Ca-ISE; DX240 Ca-ISE, perfectION™, Mettler Toledo, USA). Released Ca^{2+} are presented in respect of the total (measured by EDX) Ca content of the experimental samples.

2.4. Protein adsorption

The protein adsorption experiments were conducted using BSA (> 98%, Sigma Aldrich, USA) as a model protein. The microspheres (20 mg) was immersed in TRIS–HCl buffer of pH 7.4 ± 0.2 (5 mL) containing variable BSA concentrations (from 0 to 1 g/L). Experimental samples were incubated at 310 K for 24 h in the table-top environmental shaker-incubator under orbital shaking at 70 RPM. Then, the solution was centrifuged and the amount of BSA in the supernatants was estimated using UV–vis spectrophotometer (Evolution 300, Thermo Fisher Scientific, USA) by measuring the optical absorption on the basis of 280 nm for BSA.

2.5. Statistical analysis

The experiments were carried out in triplicate for each set of exposure. A standard error was estimated for every experimental point and marked as an error bar. It should be noted that in some cases the bars were too small to be visible.

3. Results and discussion

Theoretical and actual Mg content of the spray-dried products measured by EDX is summarized in Table 2. In general, Mg content in the products increased upon increasing an amount of Mg source in the synthesis media. It was found that not all of added Mg was incorporated into the HAp. Slight differences between theoretical and measured Mg content implies that part of Mg remain in the precursor solutions after precipitation. Furthermore, the irregular and porous samples do not allow rigorous correction of the EDX spectra. Thus, the results should be considered as semiquantitative ones [24].

FT-IR spectra of the as-dried Mg-substituted HAp microspheres (not shown) presented the characteristic vibrational bands of typical partially carbonated and hydrated apatite, as described in Refs. [6,7]. Thermal treatment did not contribute to the change of a position of $[PO_4]$ absorbance bands, while the absorbance bands characteristic to $[HPO_4]$ and $[CO_3]$ gradually disappeared. FT-IR spectra of the sintered samples displayed in Fig. 1(a) show typical absorbance bands of HAp [25]. All spectra present the bands at 562, 600, 962, 1020 and 1090 cm^{-1} related to internal vibrations, *i.e.*, symmetric stretch, bending mode, and asymmetric stretch of $[PO_4]$ tetrahedra and bands at 3573 and 630 cm^{-1} corresponding to stretching and vibrational modes of [OH], respectively. No observable differences of absorbance upon increasing Mg content were detected. However, a broadening of $[PO_4]$ absorbance bands with increasing sintering temperature occurred. Broadening of the spectra between the asymmetric stretch modes at 1020 and 1090 cm^{-1} was observed. Moreover, the absorbance decreased with increasing sintering temperature from 1173 K to 1373 K. From the XRD analyses (Fig. 1(b)), it was confirmed that a single phase HAp with maintained original crystalline structure was obtained for most of the variations. However, sintering at temperature higher than 1173 K caused an increase of β-TCP content of the 3MgHAp products as demonstrated by the presence of additional reflections in XRD patterns. This confirmed a destabilizing effect of Mg on HAp phase at high temperatures *de facto* as reported in literature [6,7,26,27].

As shown in FE-SEM micrographs (Fig. 2), the Mg-substituted HAp microspheres after sintering retained spherical shape with relatively smooth surface. No significant changes in microstructure due to increased Mg content were observed for the samples sintered at 1173 or 1273 K. However, sintering at 1373 K resulted in changes of microstructure upon increasing Mg content of the microspheres. Visual observations showed that the microspheres with higher Mg content (*i.e.*, 2MgHAp, 3MgHAp) contained considerable quantity of macropores (pores between 50 nm and 1 μm in diameter as set out by International Union of Pure and Applied Chemistry (IUPAC) [28]). Most likely, this is due to the presence of secondary phase, namely β-TCP, as revealed by XRD results. Formation of a two component system had inhibited densification. The process could be considered as transient second-phase sintering where reaction rate, namely formation of new phase is fast in comparison to densification [29].

Fig. 3(a–c) show the N_2 adsorption-desorption isotherms of the Mg-substituted HAp microspheres sintered at various tempertaures. According to the IUPAC classification, the curves are identified as type IV isotherms typically obtained in case of mesoporous adsorbents [30]. The inflection points of the isotherms indicate that the microspheres act as materials with variable pore sizes and unrestricted monolayer-multilayer adsorption of N_2 molecules. The narrow hysteresis loops is an indicative of a capillary condensation as predicted by the Kelvin equation. Moreover, in case of the sintering temperature of 1373 K, steeper upward slope at high P/P_0 (> 0.95) was observed for the samples with lower Mg content (*i.e.*, 1MgHAp) in comparison to others, as depicted in Fig. 3(c), which indicates an increase of core diameter of pores upon increasing Mg content in the bioceramic microspheres. This phenomenon could explain the similar SSA values summarized in Table 2 for the microspheres with considerably different microstructure, namely, differences between relatively dense 1MgHAp and porous 2MgHAp, 3MgHAp sintered at 1373 K. BET data are in good agreement with dilatometric curves shown at Fig. 3(d). It was evidenced that increase of Mg content supervene a two-step sintering process. For the samples labeled as 1MgHAp the shrinkage occurred in one step starting at ~873 K. Shrinkage of the samples 2MgHAp and 3MgHAp occurred in two steps. As indicated by Cacciotti et al. the differences among the samples are attributed to structural changes associated with various incorporation levels of Mg [26]. The first sintering step started at ~873 K. The higher the β-TCP content (in

Table 2
Dependence of spray-dried products SSA on Mg content and sintering temperature.

Sample designation	Theoretical Mg content, wt%	Measured Mg content, wt%	SSA before sintering, m^2/g	Sintering temperature, K	SSA after sintering, m^2/g
1MgHAp	0.34	0.31 ± 0.01	94.1 ± 9.4	1173	20.6 ± 2.1
				1273	12.0 ± 1.2
				1373	2.2 ± 0.2
2MgHAp	0.68	0.47 ± 0.02	92.4 ± 9.2	1173	23.1 ± 2.3
				1273	8.2 ± 0.8
				1373	2.4 ± 0.2
3MgHAp	1.02	0.84 ± 0.10	93.3 ± 9.3	1173	13.8 ± 1.4
				1273	5.7 ± 0.6
				1373	2.6 ± 0.3

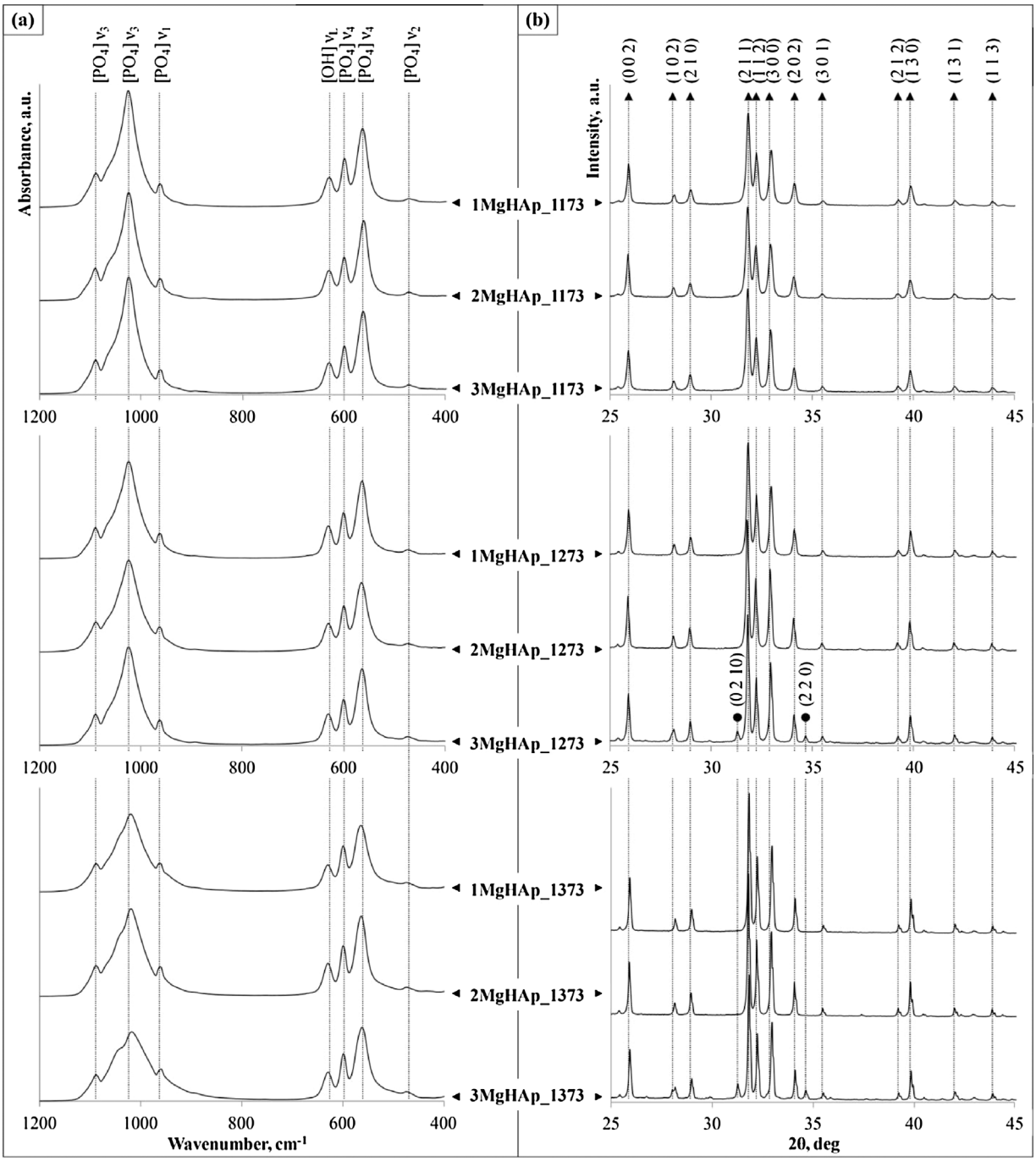

Fig. 1. (a)–FT-IR spectra and (b)–XRD patterns of Mg-substituted HAp microspheres sintered at 1173, 1273 or 1373 K (characteristic XRD peaks: ▲ – HAp; ● – β-TCP).

accordance with the XRD results), the more pronounced is the inflection point or "knee" of the dilatometric curves. The first step reached maximum shrinkage at ~1223 K and overlapped with the second step corresponding to a main densification. This phenomenon, through an enhanced sintering kinetic, promoted densification of the samples labeled as 2MgHAp and 3MgHAp up to 1350 K. Correspondingly, it caused SSA lowering of the microspheres sintered at 1173 and 1273 K upon increasing Mg content as follows: 1MgHAp → 2MgHAp → 3MgHAp (Table 2). However, subsequent rising of the temperature (over 1350 K) caused reverse effect, *i.e.*, decrease of sintering kinetics. This phenomenon reflected in the SSA values (Table 2).

No differences among SSA values of the as-dried microspheres were observed despite of various Mg content. Relatively high SSA of the as-dried microspheres is associated with slit-shaped pore structure of the nanoparticle assemblies, which are characteristic to spray-dried HAp products [31–33]. In general, three distinct categories of spray-dried particle morphology are identified, namely, crystalline, skin forming and agglomerate. The spray-dried Mg-substituted HAp products belong to the agglomerate category, which is characteristic for water-insoluble or partially soluble inorganic materials such as HAp [34]. It has been reported that the slurry composition, the ratio of the spraying air flow rate to the slurry feed rate is major factors that affect size, shape and morphology of the spray-dried products [18,31]. In this study the slurry composition as well as the spray-drying conditions were kept constant. As expected, the SSA of the products decreased upon increasing sintering temperature as grain growth and coarsening occurred (Table 2). Overall reduction of SSA values as the sintering temperature increased is attributed to the surface diffusion of atoms, resulting in coarsened

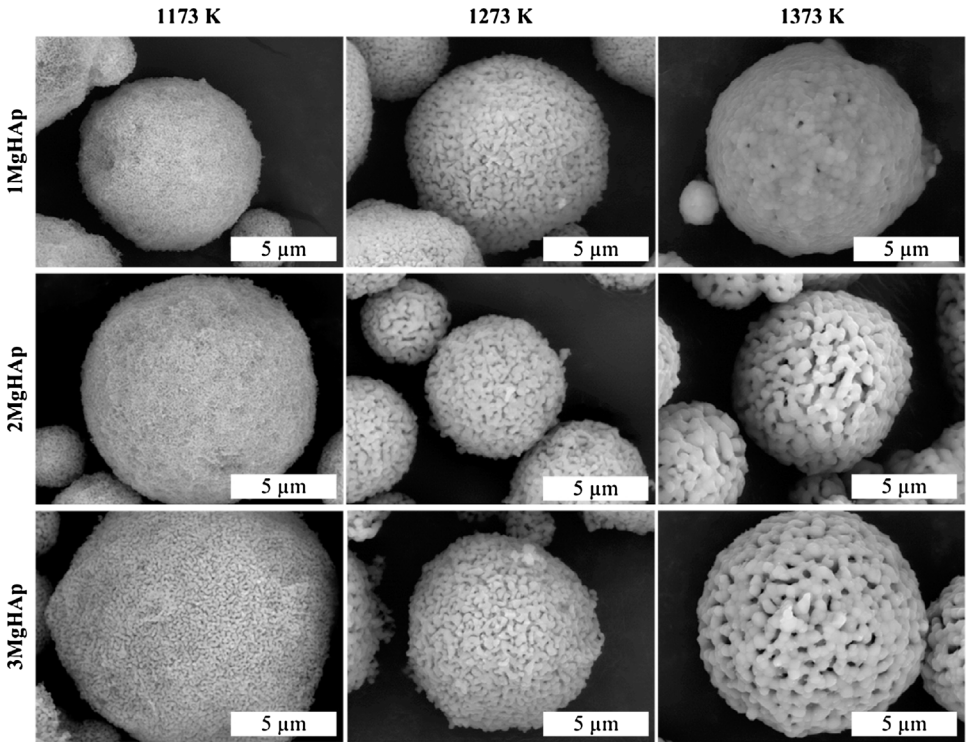

Fig. 2. FE-SEM micrographs of Mg-substituted HAp microspheres sintered at 1173, 1273 or 1373 K.

ligaments and increased pore diameters, which were confirmed by FE-SEM analysis (Fig. 2). An ambiguous link between Mg content and SSA of the bioceramic microspheres was observed. Namely, for the samples sintered at 1173 and 1273 K upon increasing Mg content SSA decreased. In case of the samples sintered at 1373 K, higher Mg content resulted in higher SSA values. Still, within standard deviations the values are rather similar. Moreover, it should be noted, that size of the microspheres varied in a relatively wide range between 2 and 16 µm (determined using FE-SEM micrographs as described in Section 2.2), which could have a significant effect on SSA measurements.

Although, SSA measurements indirectly reveal the total fraction of void space within a material, it does not address the size of the voids or their distribution. Thus, pore size distribution analysis was performed. Size of the pores present in the microspheres or the ones produced by random packing of solid particles is important for the proteins entrapment. However, due to the relatively large size and spherical shape of

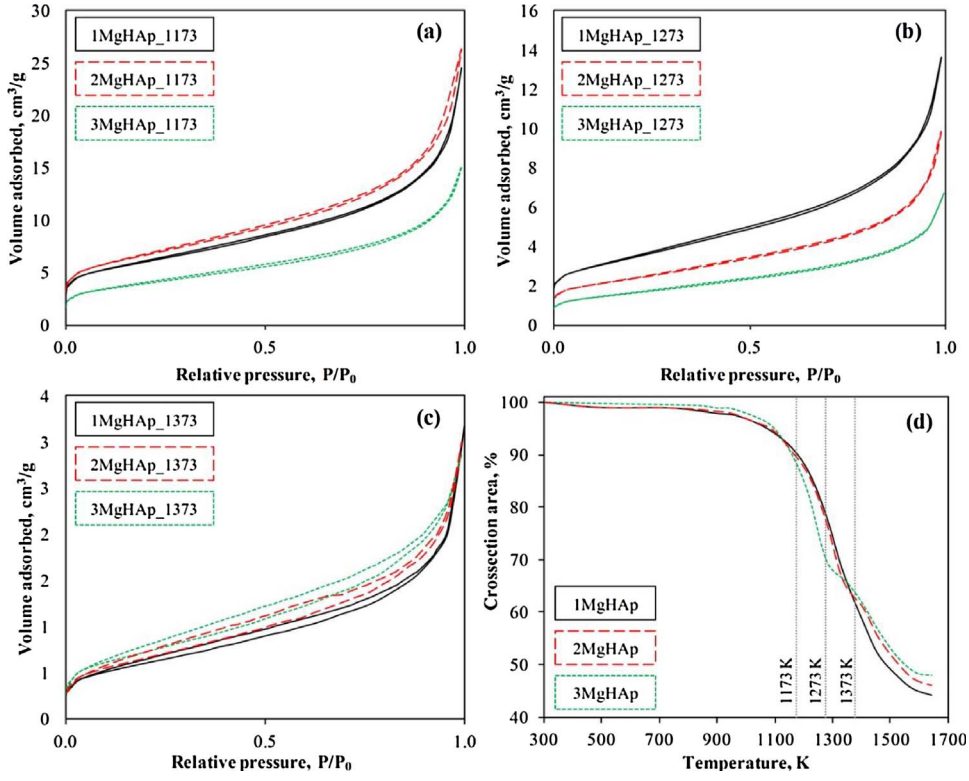

Fig. 3. (a)–(c)–N_2 adsorption-desorption isotherms and (d)–dilatometric curves of Mg-substituted HAp microspheres.

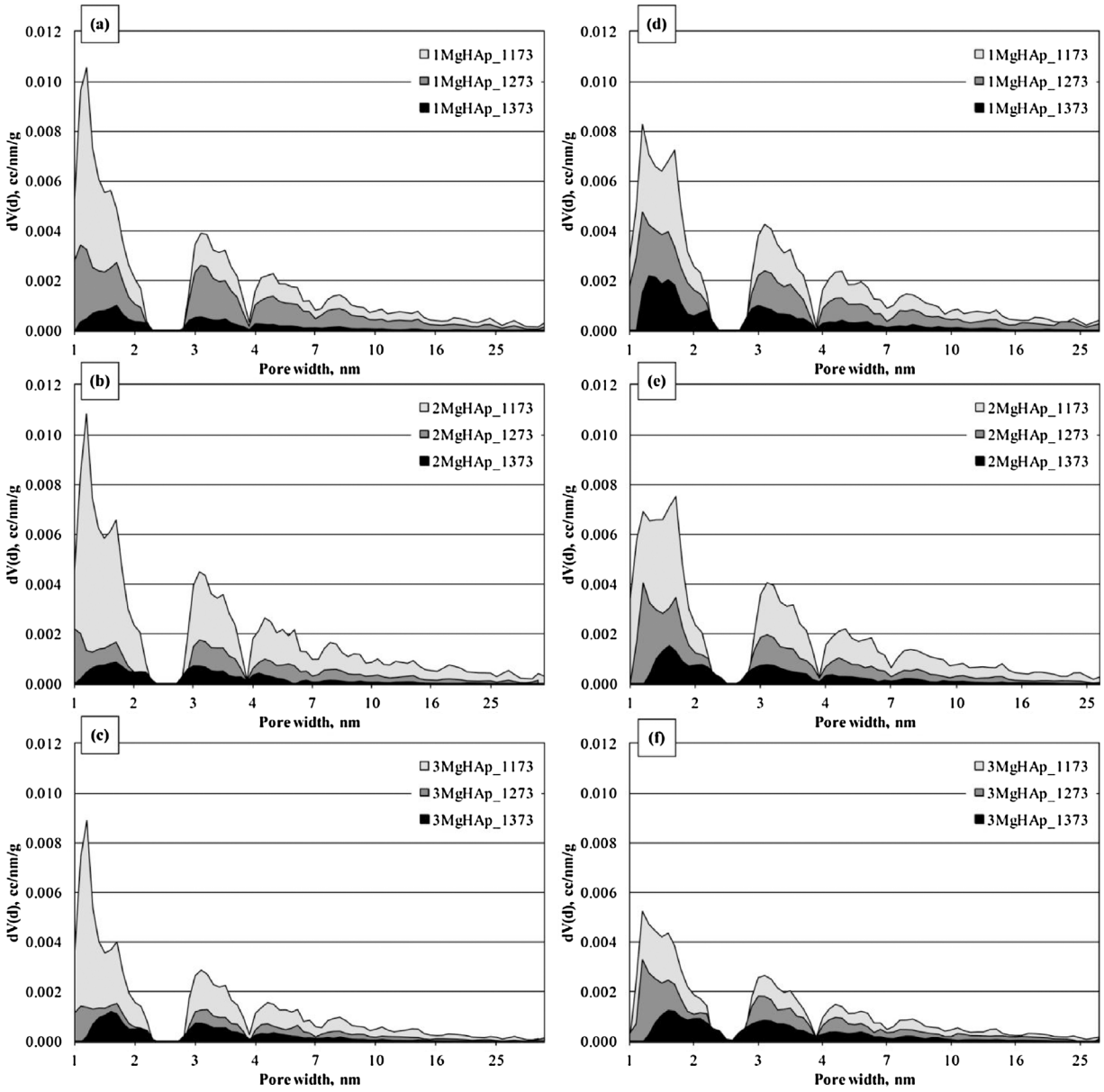

Fig. 4. Pore size distribution of Mg-substituted HAp microspheres sintered at 1173, 1273 or 1373 K: (a)–(c) before and (d)–(f) after immersion in TRIS–HCl.

the microspheres, size of the pores formed by random packing would not be comparable with that of the BSA [35]. BSA is a globular protein with the approximate shape of a prolate spheroid of dimensions 4 nm × 4 nm × 14 nm in aqueous solution [36]. Since the size of BSA is larger than the size of the micropores (up to 2 nm) and a part of mesopores (2–50 nm), the BSA could not migrate in those. Thus, the surface area for BSA adsorption of the microspheres containing large volume of the pores up to 14 nm should be downgraded. DFT adsorption cumulative pore volume of the Mg-substituted HAp microspheres is summarized in Fig. 4(a–c). The pore volume in the range of 1–30 nm considerably decreased as a result of the sintering or coarsening of the particles.

The release of Ca^{2+} from Mg-substituted HAp bioceramic microspheres was evaluated to support its bioresorbability. Moreover, the solubility is an important parameter influencing the properties of the solution and, thus, protein adsorption [23]. Ion release is presented as as-measured, (Fig. 5(a–c)) as well as normalized to surface area (Fig. 5(d–f)). For all variations the amount of Ca^{2+} released in each time point increased steadily. As expected, the ion release was conspicuously inhibited upon reduction of the surface area (Fig. 5(a–c)). Moreover, DFT adsorption cumulative pore volume measurments depicted in Fig. 4(d–f) suggest that as the microspheres dissolution progressed, the average pore size increase, namely volume of the pores smaller than 2 nm in diameter decreased. Rinsed out micro- and mesopores can further serve as channels for hydraulic flow, thus, be transformed into macropores.

The Ca^{2+} release was normalized to surface area on the grounds that it is the surface of the compounds that dissolve. It allows to evaluate the effect of Mg content on the solubility of the HAp bioceramic microspheres (Fig. 5(d, e)). In case of the samples sintered at 1173 K no differences in Ca^{2+} release were observed suggesting that there is no impact of Mg content (or it is insignificant) on Ca^{2+} release from bioceramic microspheres consisting of plain HAp phase. As illustrated in Fig. 5(e), throughout the evaluation period of 168 h Ca^{2+} release from the Mg-substituted HAp bioceramic microspheres sintered at 1273 K was higher for the samples with increased Mg content, which can be attributed to enhanced solubility of HAp phase. At the same time, an opposite phenomenon was observed for the samples sintered at 1373 K. Inhibited Ca^{2+} release from samples labeled as 3MgHAp_1373 could be attributed to higher content of β-TCP and/or Mg-substituted β-TCP as it

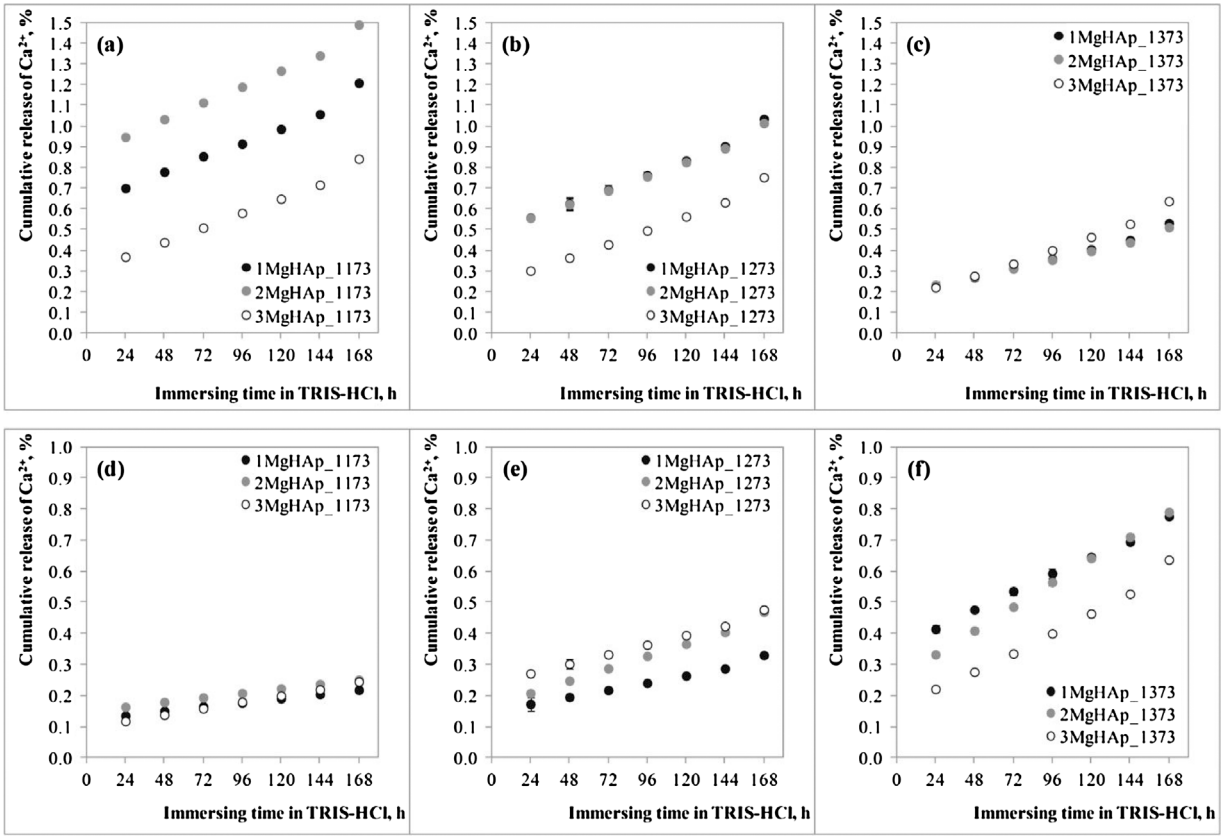

Fig. 5. Cumulative release of Ca^{2+} ions in TRIS–HCl buffer: (a)–(c) – as-measured (highlighting the effect of surface area), (d)–(f) – normalized to SSA (highlighting the effects of Mg content).

has been reported that the solubility of β-TCP decreases upon increase of Mg content [37].

The primary difference among the microspheres sintered at various temperature was the presence or absence of the micro- and mesopores, which was reflected in the SSA values (Table 2). Presence of the micro- and mesopores resulted in higher surface area, enhanced ion release and accordingly increase in the amount of BSA adsorbed on the microspheres (Fig. 6). It was found that protein sorption process fits *Langmuir* adsorption isotherm where protein molecules forms monolayer on surface [38]. The increase of the BSA concentration up to 0.5 g/L in the TRIS–HCl buffer promoted considerable increase of the adsorption capacity of all adsorbents. Upon increase of BSA initial concentration (up to 1 g/L) rather significant decrease in the amount of BSA adsorbed was observed, indicating that the number of adsorption sites (*i.e.*, Ca^{2+}) on the surfaces of the microspheres limited the adsorption capacity. Although the results suggest that SSA is a major contributor to protein adsorption, significant influence of the Mg content was found. The SSA of the samples labeled as 1MgHAp_1273 ($8.2 \pm 0.8\ m^2/g$) was lower in comparison to 3MgHAp_1173 ($13.8 \pm 1.4\ m^2/g$), still the BSA adsorbed was twice as high (at BSA initial concentration 1 g/L). According to literature, the differences in BSA adsorption caused by Mg incorporation could be attributed to the difference in protein bonding sites distribution, namely, decrease of Ca^{2+} sites on the microspheres surfaces [23,39]. The correlation between Ca^{2+} release and protein adsorption was observed. The amount of the BSA adsorbed on the microspheres decreased as the Ca^{2+} release decreased (Fig. 5(a–c)) as follows: 1MgHAp_1173 → 1MgHAp_1273 → 3MgHAp_1273 → 1MgHAp_1373 → 3MgHAp_1373. It has been reported, that protein exposes more polar-ionized residues to the solvent due to higher ionic strength of the media, thus, interaction between protein and the surface-binding sites, *i.e.*, Ca^{2+}, is enhanced [40].

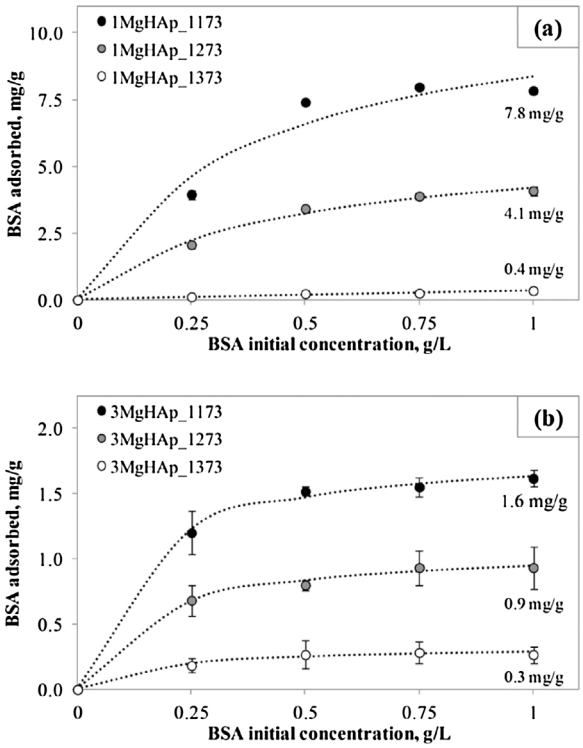

Fig. 6. The BSA adsorption capacity of Mg-substituted HAp bioceramic microspheres *versus* initial protein concentration in TRIS–HCl buffer: (a) 1MgHAp and (b) 3MgHAp.

4. Conclusions

The objective of this study was to elucidate the importance and connection between surface physicochemical characteristics and solubility with the adsorption of proteins on Mg-substituted HAp microspheres. For this purpose, porous HAp bioceramic microspheres containing up to 0.84 ± 0.10 wt% were obtained by spray drying at 353 ± 5 K and subsequent sintering at 1173, 1273 or 1373 K. Increase of Mg content supervene a two-step sintering process of HAp, which cause reduction of SSA upon increasing Mg content of the microspheres sintered at 1173 or 1273 K and reverse effect when the microspheres are sintered at 1373 K. The results indicated that presence of micro- and mesopores effectively enhance the solubility, namely Ca^{2+} ion release, and increase the amount of BSA adsorbed on the microspheres. The amount of BSA uptake was found to be the highest (7.8 mg/g) for HAp bioceramic microspheres with the lowest Mg content. Namely increase of Mg content significantly alter the protein adsorption capacity. Thus, it is feasible to use the HAp bioceramic microspheres as protein carries by incorporation of Mg with predesigned parameters for particular therapeutic effect.

Acknowledgements

Support for this work was provided by the Riga Technical University through the Scientific Research Project Competition for Young Researchers No. ZP-2017/2 and by the National Research Programme No. 2014.10-4/VPP-3/21 “MultIfunctional Materials and composItes, photonicS and nanotechnology (IMIS2)” Project No. 4 “Nanomaterials and nanotechnologies for medical applications.”

References

[1] L.L. Hench, Bioactive materials: the potential for tissue regeneration, J. Biomed. Mater. Res. 41 (1998) 511–518.
[2] W. Habraken, P. Habibovic, M. Epple, M. Bohner, Calcium phosphates in biomedical applications: materials for the future? Mater. Today 19 (2) (2016) 69–86.
[3] B.T. Wopenka, J.D. Pasteris, A mineralogical perspective on the apatite in bone, Mater. Sci. Eng. C 25 (2005) 131–143.
[4] V. Mouriño, J.P. Cattalini, A.R. Boccaccini, Metallic ions as therapeutic agents in tissue engineering scaffolds: an overview of their biological applications and strategies for new developments, J. R. Soc. Interface 9 (68) (2012) 401–419.
[5] M. Supova, Substituted hydroxyapatites for biomedical applications: a review, Ceram. Int. 41 (2015) 9203–9231.
[6] L. Stipniece, K. Salma-Ancane, N. Borodajenko, M. Sokolova, D. Jakovlevs, L. Berzina-Cimdina, Characterization of Mg-substituted hydroxyapatite synthesized by wet chemical method, Ceram. Int. 40 (2014) 3261–3267.
[7] L. Stipniece, I. Narkevica, K. Salma-Ancane, Low-temperature synthesis of nanocrystalline hydroxyapatite: effect of Mg and Sr content, J. Am. Ceram. Soc. 100 (2017) 1697–1706.
[8] L. Robinson, K. Salma-Ancane, L. Stipniece, B.J. Meenan, A.R. Boyd, The deposition of strontium and zinc co-substituted hydroxyapatite coatings, J. Mater. Sci. Mater. Med. 28 (3) (2017) 51 1–14.
[9] A. Dubnika, D. Loca, I. Salma, A. Reinis, L. Poca, L. Berzina-Cimdina, Evaluation of the physical and antimicrobial properties of silver doped hydroxyapatite depending on the preparation method, J. Mater. Sci. Mater. Med. 25 (2) (2014) 435–444.
[10] E. Boanini, M. Gazzano, A. Bigi, Ionic substitutions in calcium phosphate synthesized at low temperature, Acta Biomater. 6 (6) (2010) 1882–1894.
[11] M.J. Laires, C.P. Montmeiro, M. Bicho, Role of cellular magnesium in health and human disease, Front. Biosci. 9 (2014) 262–276.
[12] L. Wu, B.J.C. Luthringer, F. Feyerabend, A.F. Schilling, R. Willumeit, Effects of extracellular magnesium on the differentiation and function of human osteoclasts, Acta Biomater. 10 (6) (2014) 2843–2854.
[13] H. Zreiqat, C.R. Howlett, A. Zannettino, P. Evans, G. Schulze-Tanzil, C. Knabe, M. Shakibaei, Mechanisms of magnesium-stimulated adhesion of osteoblastic cells to commonly used orthopaedic implants, J. Biomed. Mater. Res. A 62 (2002) 175–184.
[14] S. Adzila, M.C. Murad, I. Sopyan, Doping metals into calcium phosphate phase for better performance of bone implant materials, Recent Pat. Mater. Sci. 5 (2012) 18–47.
[15] H.D. Nguea, B. Rihn, D. Mahon, J.L. Bernard, A. De Reydellet, A. Le Faou, Effects of various man-made mineral fibers on cell apoptosis and viability, Arch. Toxicol. 79 (2005) 487–492.
[16] D. Loca, J. Locs, A. Dubnika, V. Zalite, L. Berzina-Cimdina, Porous hydroxyapatite for drug delivery, in: M. Mucalo (Ed.), Hydroxyapatite (HAp) for Biomedical Applications, Elsevier Ltd., 2015, pp. 129–142.
[17] F. Barrere-de Groot, C.A. van Blitterswijk, K. de Groot, Bone regeneration: molecular and cellular interactions with calcium phosphate ceramics, Int. J. Nanomed. 1 (3) (2006) 317–332.
[18] R. Cholas, S.K. Padmanabhan, F. Gervaso, G. Udayan, G. Monaco, A. Sannino, A. Licciulli, Scaffolds for bone regeneration made of hydroxyapatite microspheres in a collagen matrix, Mater. Sci. Eng. C 3 (2016) 499–505.
[19] A. Wang, Y. Lu, R. Zhu, S. Li, X. Ma, Effect of process parameters on the performance of spray dried hydroxyapatite microspheres, Powder Technol. 191 (1–2) (2009) 1–6.
[20] High-Resolution Protein Separations Using CHT Ceramic Hydroxyapatite. Bulletin 1842, Bio-Rad Laboratories. Web site: http://www.bio-rad.com, USA.
[21] P. Luo, T.G. Nieh, Preparing hydroxyapatite powders with controlled morphology, Biomaterials 17 (1996) 1959–1964.
[22] T.S.S. Kumar, K. Madhumathi, B. Rajkamal, S. Zaheatha, A.R. Malar, S.A. Bai, Enhanced protein delivery by multi-ion containing eggshell derivedapatitic-alginate composite nanocarriers, Colloids Surf. B: Biointerfaces 123 (2014) 542–548.
[23] K. Wang, C. Zhou, Y. Hong, X. Zhang, A review of protein adsorption on bioceramics, Interface Focus 2 (2012) 259–277.
[24] A. Wassilkowska, A. Czaplicka-Kotas, M. Zielina, A. Bielski, An analysis of the elemental composition of micro-samples using EDS technique, Tech. Trans. Chem. 1-Ch (2014) 133–148.
[25] L. Berzina-Cimdina, N. Borodajenko, Research of calcium phosphates using Fourier transform infrared spectroscopy, in: T. Theophile (Ed.), Infrared Spectroscopy – Materials Science, Engineering, and Technology, InTech, Rijeka, 2012510 p..
[26] A. Cacciotti, A. Bianco, M. Lombardi, L. Montanaro, Mg-substituted hydroxyapatite nanopowders: synthesis, thermal stability and sintering behavior, J. Eur. Ceram. Soc. 29 (2009) 2969–2978.
[27] W.L. Suchanek, K. Byrappa, P. Shuk, R.E. Riman, V.F. Janas, K.S. Ten-Huisen, Preparation of magnesium-substituted hydroxyapatite powders by the mechanochemical hydrothermal method, Biomaterials 25 (2004) 4647–4657.
[28] International Union of Pure and Applied Chemistry Physical Chemistry division commission on colloid and surface chemistry, subcommittee on characterization of porous solids, recommendations for the characterization of porous solids (technical report), Pure Appl. Chem. 66 (8) (1994) 1739–1758.
[29] L.C. De Jonghe, M.N. Rahaman, Sintering of ceramics, Handbook of Advanced Ceramics, Elsevier, New York, 2003.
[30] Y.-P. Guo, Y.-B. Yao, Y.-J. Guo, C.-Q. Ning, Hydrothermal fabrication of mesoporous carbonated hydroxyapatite microspheres for a drug delivery system, Microporous Mesoporous Mater. 155 (2012) 245–251.
[31] W. Sukaraseraneel, S. Watcharamaisakul1, B. Golman, J. Suwanprateeb, Effect of process parameters on characteristics of spray-dried hydroxyapatite granules, Key Eng. Mater. 728 (2017) 341–346.
[32] L. Stipniece, K. Salma-Anacane, I. Narkevica, I. Juhnevica, L. Berzina-Cimdina, Fabrication of nanostructured composites based on hydroxyapatite and ε-polylysine, Mater. Lett. 163 (2016) 65–68.
[33] L. Stipniece, K. Salma-Ancane, V. Rjabovs, I. Juhnevica, M. Turks, I. Narkevica, L. Berzina-Cimdina, Development of functionalized hydroxyapatite/poly(vinyl alcohol) composites, J. Cryst. Growth 444 (2016) 14–20.
[34] D.E. Walton, C.J. Mumford, Spray dried products-characterization of particle morphology, Chem. Eng. Res. Des. 77 (1) (1999) 21–38.
[35] E. Fujii, M. Ohkubo, K. Tsuru, S. Hayakawa, A. Osaka, K. Kawabata, C. Bonhomme, F. Babonneau, Selective protein adsorption property and characterization of nanocrystalline zinc-containing hydroxyapatite, Acta Biomater. 2 (2006) 69–74.
[36] H.T.M. Phan, S. Bartelt-Hunt, K.B. Rodenhausen, M. Schubert, J.C. Bartz, Investigation of bovine serum albumin (BSA) attachment onto self-assembled monolayers (SAMs) using combinatorial quartz crystal microbalance with dissipation (QCM-D) and spectroscopic ellipsometry (SE), PLoS One 10 (10) (2015) e0141282.
[37] C. Tardei, F. Grigore, I. Pasuk, S. Stoleriu, The study of Mg2+/Ca2+ substitution of beta-tricalcium phosphate, J. Optoelectron. Adv. Mater. 8 (2008) 568–571.
[38] X.-Y. Zhao, Y.-J. Zhu, F. Chen, B.-Q. Lu, J. Wu, Nanosheet-assembled hierarchical nanostructures of hydroxyapatite: surfactant-free microwave hydrothermal rapid synthesis, protein/DNA adsorption and pH-controlled release, CrystEngComm 15 (2013) 206–212.
[39] T. Tonegawa, T. Ikoma, T. Yoshioka, G. Chen, N. Hanagata, J. Tanaka, Characterization and protein adsorption ability of zinc iron and magnesium hydroxyapatite, Key Eng. Mater. 361–363 (2008) 187–190.
[40] D.T.H. Wassell, R.C. Hall, G. Embery, Adsorption of bovine serum albumin onto hydroxyapatite, Biomaterials 16 (1995) 697–702.